

Synthesis and Characterization of Calcium and Tin Co-Doped Barium Titanate ($\text{Ba}_{0.91}\text{Ca}_{0.09}\text{Sn}_{0.01}\text{Ti}_{0.99}\text{O}_3$) Ceramic Using Solid State Synthesis for Energy Storage Application in Ceramic Capacitor

¹T.O. Daniel*, ¹L.C. Okafor, ¹J.U. Arikpo, ²E. Udeh, ³O.D. Shaibu,
⁴G.O. Edaogbogun and ¹P.E. Okobi ⁴O.K. Olawale

¹Department of Physics, Alex Ekwueme Federal University Ndufu-Alike, Nigeria.

²Department of Physics and Astronomy, University of Kansas, United States of America.

³Department of Electrical Engineering, University of Buffalo, New York 14260, USA.

⁴Department of Physics, Federal Polytechnic, Ede, Osun State, Nigeria.

danieljonugwathomas@gmail.com, daniel.thomas@funai.edu.ng*

(Received on 26th June 2024, accepted in received form 24th April 2024)

Summary: The lead content in piezoelectric ceramic (lead-zirconate-titanate) capacitors is a major draw back due to its hazardous nature. As a result, alternate materials must be sought. The $\text{Ba}_{0.91}\text{Ca}_{0.09}\text{Sn}_{0.01}\text{Ti}_{0.99}\text{O}_3$ (BCST) ceramic was synthesized via solid-state synthesis and studied via energy dispersive spectroscopy, scanning electron microscopy, X-ray diffraction, Fourier transform infrared spectroscopy, and dielectric measurements for use in ceramic capacitors. The BCST ceramic EDS spectrum confirmed Ca, Ba, O, Sn and Ti, as well as a trace quantity of C, Au, and Pd impurities. As determined by ImageJ, the SEM image shows grains of inhomogeneous shape and porosity with a nonuniform distribution of grains and an average grain size of 1.64 μm . The XRD results show that a crystalline ceramic with a tetragonal perovskite structure and an average crystalline size of 26.35 nm exists. The evolution of the FTIR and dielectric behavior reveals the presence of two phase transitions, T_{R-O} and T_{O-T} (tetragonal-orthorhombic phase transition at 150°C and orthorhombic-tetragonal phase transition at 500°C), as well as a dielectric constant relaxation behavior that makes it suitable for use in ceramic capacitors. The properties obtained are suitable for the manufacture of multilayer ceramic capacitors using $\text{Ba}_{0.91}\text{Ca}_{0.09}\text{Sn}_{0.01}\text{Ti}_{0.99}\text{O}_3$.

Keywords: Barium titanate, Ceramics, Capacitor, Solid-state synthesis, Dielectric.

Introduction

The growing demand for lead-free piezoelectric materials in ceramic capacitors has driven research into barium Titanate (BaTiO_3 , BTO)-based ceramics. While lead Zirconate Titanate (PZT) dominates capacitor applications due to its high dielectric constant, its toxicity and environmental risks necessitate alternatives. BTO, a perovskite ferroelectric, offers eco-friendliness but suffers from low piezoelectric coefficients and structural instability at elevated temperatures. Recent studies on doped BTO (e.g., $\text{Ca}^{2+}/\text{Sn}^{4+}$ co-doping) highlight improved dielectric relaxation and thermal stability, addressing these limitations [1, 2]. Solid-state synthesis remains the industry-preferred method for scalable ceramic production due to its cost-effectiveness and reproducibility [3].

Single crystals of barium titanate can be produced from molten potassium fluoride at a temperature of approximately 1100°C [4]. BaTiO_3 possesses a ferroelectric perovskite tetragonal phase from ambient temperature to the Curie temperature (T_c) before converting into a paraelectric-cubic phase. The use of pure BaTiO_3 in piezoelectric devices has several

drawbacks, such as structural phase transitions at low temperatures and poor piezoelectric constants, which limits its widespread application [3, 5].

All capacitors, sensors, actuators, and resistors use piezoelectric materials as dielectrics [6-7]. Lead Titanate (PbTiO_3) was among the first piezoelectric ceramics discovered, but its toxicity led to the exploration of eco-friendly alternatives like BaTiO_3 [7]. Titanate are members of the perovskite family of minerals and are naturalized structures composed of several oxides with the chemical formula ABO_3 [8-9]. Zinc oxide, aluminium nitride, barium-titanate oxide, and lead-zirconate-titanate (PZT) oxides are examples of piezoelectric materials. Because of its extensive technological applications, PZT is the most commonly used piezoelectric ceramic [5]. Barium titanate-based electro ceramics are among the prevalent ferroelectric materials, with widespread application as dielectric materials for multilayer ceramic capacitors and embedded capacitance in printed circuits due to their high dielectric constant, low loss and thermal stability.

*To whom all correspondence should be addressed.

Due to its high lead content, PZT has one main disadvantage: because lead is released into the atmosphere during processing, it is dangerous [5]. Poisonous materials have the potential to harm the brain and nervous system [10-11]. A wide range of systems that are free of lead have been studied, and several have shown characteristics similar to those of PZT. BaTiO₃ has been identified as a potential material. BaTiO₃ is a perovskite oxide ferroelectric with a significant dielectric constant at its T_c temperature [2, 6, 12]. However, issues, such as the strain's high hysteresis and the material's field of electricity dependency, which make control difficult, and a low piezoelectric constant, prevent the widespread use of pure BaTiO₃ [6, 13]. The doping of BaTiO₃ will enhance the production of the hexagonal phase, according to various studies [14-15]. By lowering the dielectric constant and shifting the phase transition temperature from low to high, the Fe-substituted BaTiO₃ ceramic (BTF) for example decreases the dielectric properties of the latter [14-15]. The high dielectric constant and its behaviour are important factors in the application of doped barium titanate [16].

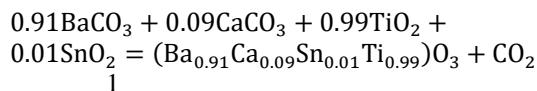
This research investigates Ca/Sn co-doped BTO to enhance energy storage performance in multilayer ceramic capacitors (MLCCs), leveraging synergies between defect engineering and phase stabilisation. Doping BaTiO₃ with Ca²⁺ and Sn⁴⁺ will enhance its dielectric properties, making it ideal for capacitor applications. Ca²⁺ substitutes Ba²⁺ in the A-site, improving thermal stability and reducing domain wall motion, while Sn⁴⁺ replaces Ti⁴⁺ in the B-site, increasing dielectric permittivity and enhancing relaxor behavior. This modification stabilizes the dielectric response across temperature variations, reduces dielectric loss, and lowers the Curie temperature, making it suitable for multilayer ceramic capacitors (MLCCs) in high-performance electronic applications such as power electronics and telecommunications.

Experimental

A digital electronic balance (Mettler Toledo XS205 Dual Range balance (±0.01 mg accuracy)) was used to weigh stoichiometric amounts of analytical grade BaCO₃ (Sigma-Aldrich, 99.9%), TiO₂ (Merck, 99.5%), CaCO₃ (Merck, 99%), SnO₂ (Fisher Scientific, 99.9%) (starting powders/raw materials). The weighed powders were dry mixed, and then wet mixed with distilled water and baked at 200 °C in an oven for 1 hour. For four hours, the dried material was hand-crushed for homogeneity using a mortar and pestle. Next, the homogeneous mixture was placed in a crucible made of alumina and calcined at 1100 °C for four hours in a furnace (Nabertherm muffle furnace with ±5 °C temperature control and a heating rate of 5 °C/min to ensure

uniformity) to enable volatilization of the CO₂ by-product. The calcined powder was reground for approximately one hour with 4 wt% polyvinyl alcohol (PVA) added as a binder to improve the compactness of the material grains. PVA binder (4 wt%, Sigma Aldrich) was homogenized via 30-minute ball milling to ensure compactness. Post-sintering

At a pressure of 10 tons using Hydraulic press (Carver Auto Series), pellets with diameters of 26 mm and thicknesses of 1 mm were produced. The pellets were then sintered at 1100 °C for three hours before being cooled to allow the crystal phase to form. The stoichiometric quantities of the raw materials according to the supplied equation regulated the doping site of Ca and Sn ions in BaTiO₃, as expressed in equation 1.



A scanning electron microscope (Hitachi SU8010 (5 kV accelerating voltage, Au-Pd coating)) was used to examine the microstructure of the ceramic material. The equipment was run at a 40 kV accelerating voltage, while the photos were taken at a 5 kV voltage. The samples were backed onto an aluminum stage with carbon adhesive tape. Because the samples were not conductive, a sputter coater was used to coat them in a thin layer of AuPd. The samples were inserted into the chamber with an exchange rod and held in an SEM holder. The peaks in all of the elemental composition spectra of the samples were then analysed and identified, and images were captured at the desired magnification. An X-ray diffractometer (D8 Advance, Bruker AXS, 40 kV, 40 mA) was used to measure the crystal structure, space group, crystal size, and lattice parameters at room temperature using monochromatic CuK (= 1.540598). After identifying the background and peak positions, a search-matched method was run using the intensities and peak positions. Origin Pro 2018 was used to create the XRD diffractogram. By producing an infrared absorption spectrum, an Agilent Fourier transform infrared (FTIR) machine model Happ-Genzel was utilized to determine the chemical bonding in the ceramic. The dielectric characteristics as a function of temperature were investigated with an Agilent E4980A Precision LCR meter from 20 Hz to 2 MHz.

Results and Discussion

Stoichiometry Analysis/Energy Dispersive Spectroscopy (EDS)

The chemical composition of the BCST ceramic is shown in Fig 1 by the EDS spectrum (Ba_{0.91}Ca_{0.09}Sn_{0.01}Ti_{0.99}O₃). The presence of O, Ba, C, Ca, Sn, Ti, Pd and Au in the BCST ceramic spectrum was

quantified and is reported in Table 1. Fig 1 shows that the substance contains carbon (C) and gold-palladium (AuPd). The carbon might be attributed to the carbon tape background, whereas the Au and Pd present could be a result of the sample coating prior to conduction characterization. No further impurity peaks, however, were found.

Table-1: Atomic ratio of the nominal composition of the BCST ceramics.

Sample	Atomic ratio		
	Ba/Ca	Ti/Sn	O
Nominal	6.98	38.02	59
BCST	4.63	65.6	46.95

The quantification results for the $\text{Ba}_{0.91}\text{Ca}_{0.09}\text{Sn}_{0.01}\text{Ti}_{0.9}\text{O}_3$ ceramics are shown in Table-1. However, because there is considerable overlap between Sn and Ca and between Ba and Ti, it is possible that the findings for Ba are more likely to be Ti and that Ca is more likely to be Sn or vice versa. Table 1 provides a way to compare the atomic ratios of the nominal and normalized EDS-determined compositions.

Scanning electron microscopy (SEM)

Fig 2 shows the surface morphology of $\text{Ba}_{0.91}\text{Ca}_{0.09}\text{Sn}_{0.01}\text{Ti}_{0.9}\text{O}_3$ as studied by SEM. Using ImageJ, the average grain size of the sample was computed [17-19].

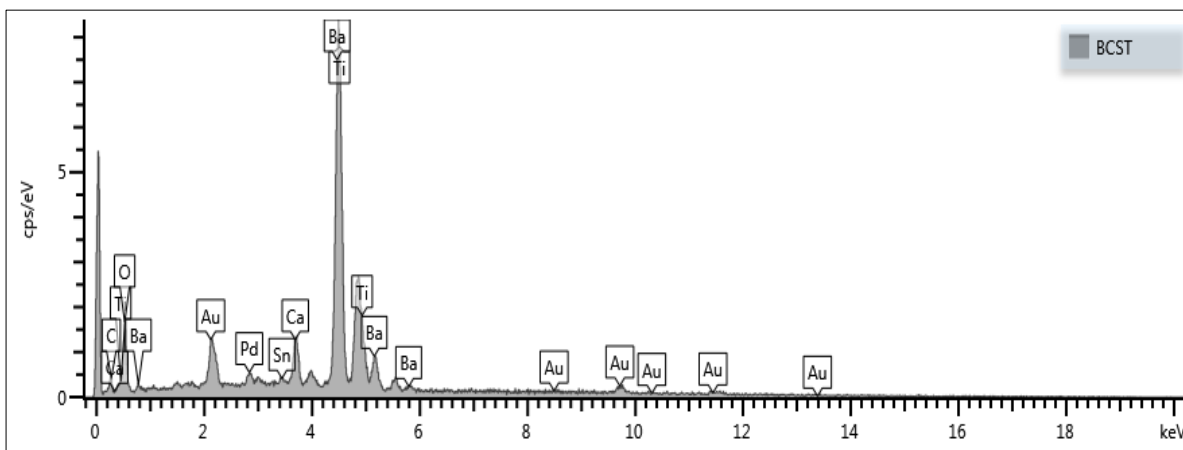
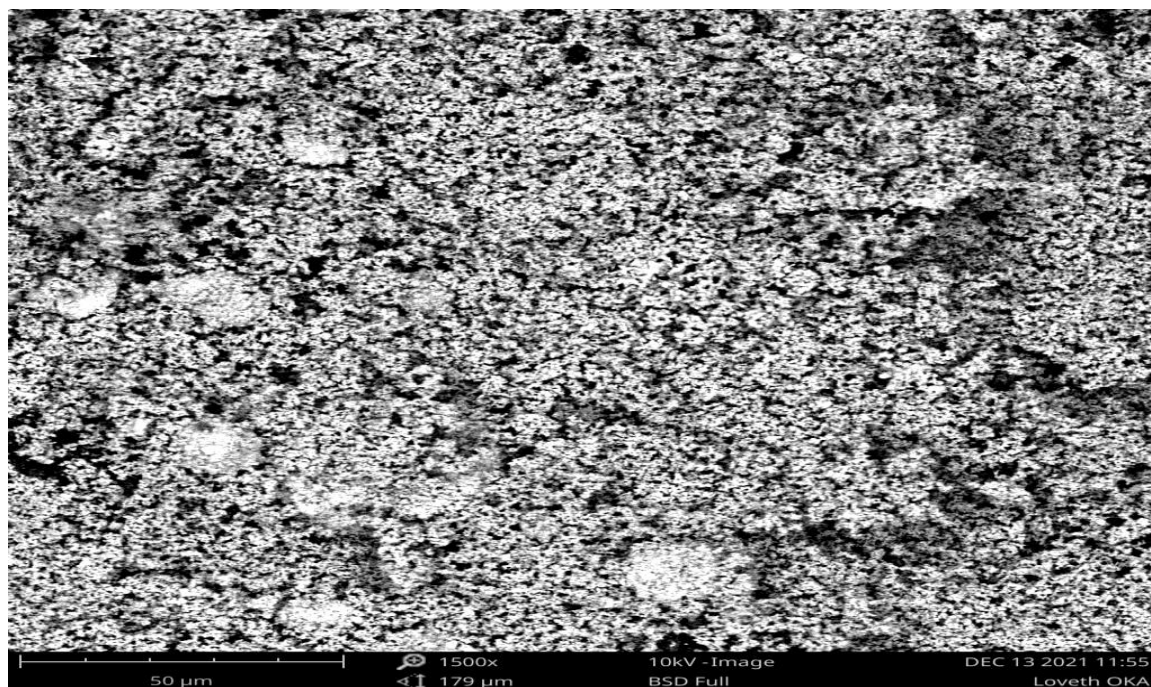


Fig 1: EDS spectrum of the $\text{Ba}_{0.91}\text{Ca}_{0.09}\text{Sn}_{0.01}\text{Ti}_{0.9}\text{O}_3$ ceramic.



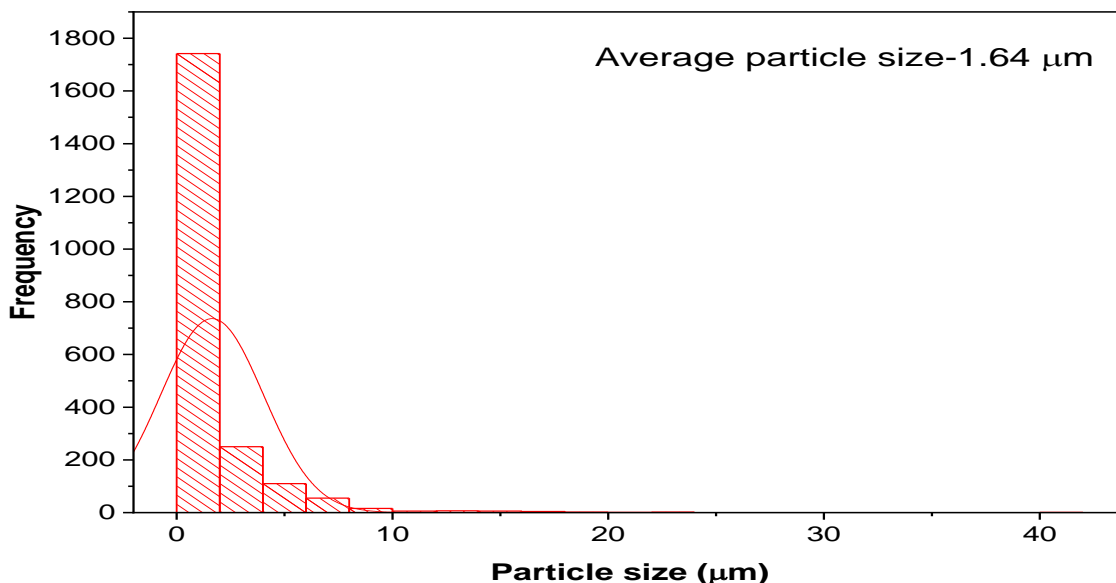


Fig. 2: Surface morphology of $Ba_{0.91}Ca_{0.09}Sn_{0.01}Ti_{0.9}O_3$ and particle size distribution.

In the SEM micrographs, the grains have a somewhat inhomogeneous shape and porosity, as well as a non-uniform distribution of grains and the coexistence of tiny and large grains, indicating that the addition of Sn causes irregular grain growth in the $Ba_{0.91}Ca_{0.09}Sn_{0.01}Ti_{0.9}O_3$ ceramic. A few grains clump together, and there is a fine-grained microstructure with unclear grain boundaries and a few rod-like grains. The average grain size was estimated to be 1.64 μm , which is lower than that found in normal barium titanate ceramics manufactured at higher temperatures [13, 20]. The presence of rod-like grains could be explained by the non-uniform distribution of the composition [21].

X-ray diffraction (XRD) analysis of $Ba_{0.91}Ca_{0.09}Sn_{0.01}Ti_{0.9}O_3$ (BCST)

The XRD pattern of the synthesized $Ba_{0.91}Ca_{0.09}Sn_{0.01}Ti_{0.9}O_3$ (BCST) ceramics is shown in Fig 3. The XRD pattern shows that the ceramic is crystalline with a tetragonal perovskite structure, which matches the reference card JCPDS no: 00-005-

0626 for $BaTiO_3$ (Fig 4). However, a modest peak with extremely low intensity was observed at 2θ values of approximately 23.24° and 33.14° . The orthorhombic $CaTiO_3$ phase was observed as a peak (JCPDS file no:00-022-0153).

The Scherrer equation was used to determine the average crystallite size of the $Ba_{0.91}Ca_{0.09}Sn_{0.01}Ti_{0.9}O_3$ ceramic to be 26.35 nm, which is listed in Table 2 along with the d-spacing, full width half maximum, and microstrain derived from the most favourable peak at a 200 miller index using applicable formulae. The minor orthorhombic $CaTiO_3$ phase (Fig. 3) introduces compressive strain at grain boundaries, enhancing mechanical stability and reducing leakage currents. Similar secondary phases in Nd-doped $BiFeO_3$ [22] were shown to improve dielectric breakdown strength, suggesting analogous benefits here. However, excessive secondary phases may fragment the perovskite matrix, necessitating future doping optimization

Table-2: Peak position, FWHM, d spacing, crystallite size and microstrain of $Ba_{0.91}Ca_{0.09}Sn_{0.01}Ti_{0.9}O_3$ at (200).

Sample	2θ (degree)	FWHM (degree)	d (Å)	Average Crystallite Size (nm)	Microstrain ($\epsilon \times 10^{-3}$)
BCST	45.261	0.410	2.00189	26.35	3.2

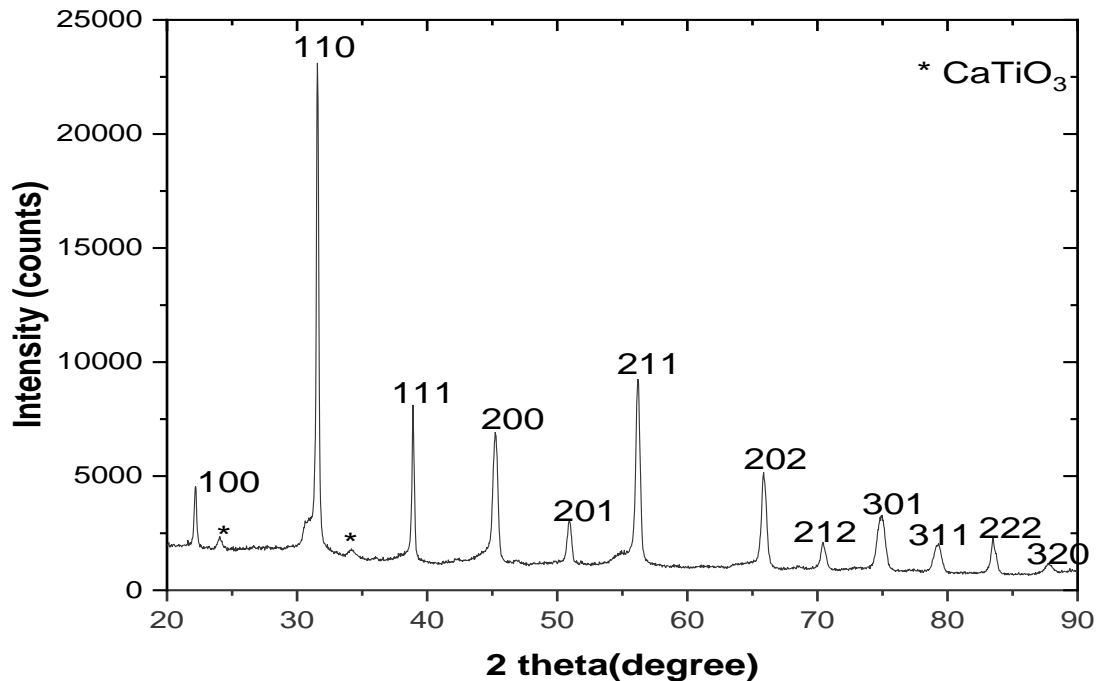


Fig. 3: XRD pattern for Ba_{0.91}Ca_{0.09}Sn_{0.01}Ti_{0.9}O₃.

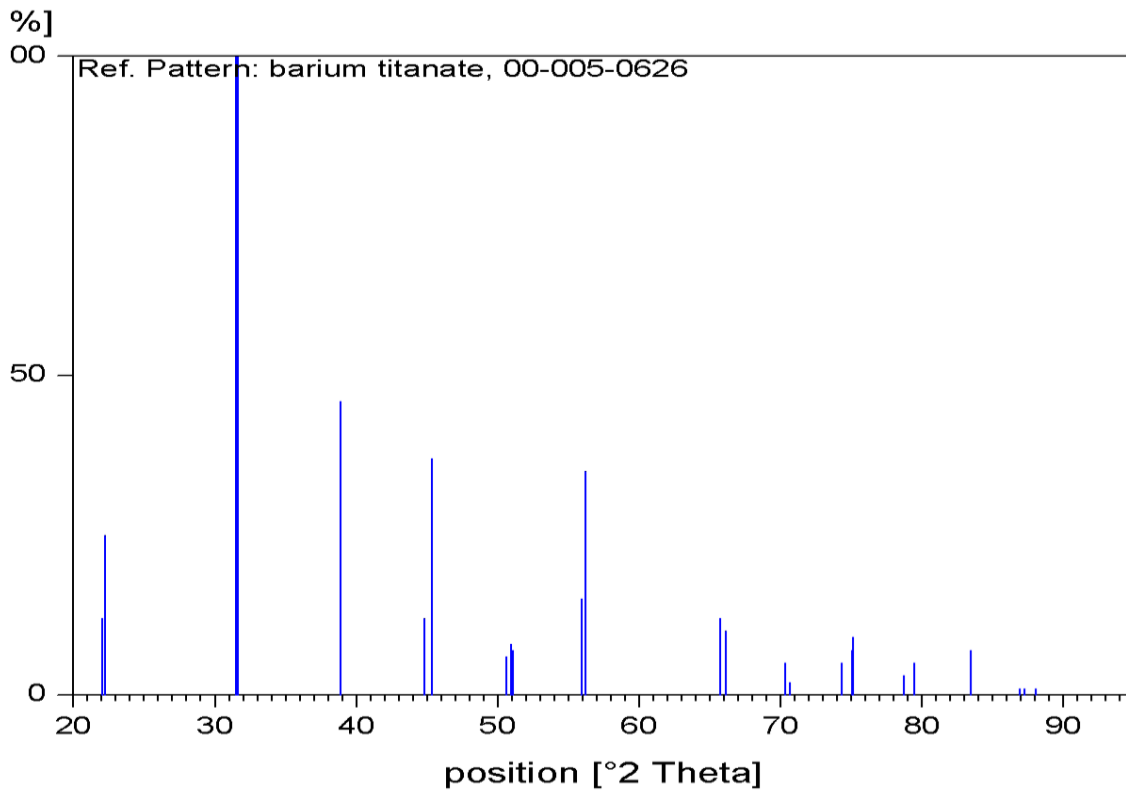


Fig. 4: JCPDS no. 00-005-0626 crystal pattern of BaTiO₃.

The lattice constants of the $\text{Ba}_{0.91}\text{Ca}_{0.09}\text{Sn}_{0.01}\text{Ti}_{0.9}\text{O}_3$ ceramic were calculated using the XRD diffractogram, where the tetragonal phase aspect ratio of the lattice, $c/a = 1.0022$, is advantageous because it promotes polarizability and improves the ferroelectric characteristics of the ceramic, defining its application [23]. The slight tetragonal distortion increases spontaneous polarization by elongating the Ti-O bond along the c-axis, enhancing polarizability. This is critical for ferroelectric hysteresis, where higher c/a ratios correlate with superior energy density in MLCCs [24]. Comparatively, Sm-doped double perovskites [25] show similar trends, validating our findings.

Fourier Transform Infrared Spectroscopy

Fig 5 shows the FTIR spectrum of the $\text{Ba}_{0.91}\text{Ca}_{0.09}\text{Sn}_{0.01}\text{Ti}_{0.9}\text{O}_3$ ceramic. The calcium and tin dopants alter the crystal structure, causing the relative vibration of the crystal lattice to be influenced by interactions between different metallic ions in the

material. FTIR characterization was used to explore this impact. At wavenumbers of 1021.3, 1066.0, 1446.2, 2165.6, and 2363.13 cm^{-1} , characteristic bands were observed. The C=O stretching mode of an ester bond corresponds to the absorption modes at 1021.3 cm^{-1} and 1066.0 cm^{-1} . When the Ti-O bonds were strengthened, the corresponding absorption peaks moved to greater wavenumbers. The FTIR peak shift to higher wavenumbers (1021–1066 cm^{-1}), indicates shorter Ti-O bond lengths due to Sn/Ca doping and increasing bond strength. This strengthens the perovskite framework, reducing ionic mobility losses, as observed in Cu-doped perovskite-polymer composites [26].

The ionic bond, which could be derived from carbonate precursors, is represented by the 1446.2 cm^{-1} band. The O-H stretching vibration mode is ascribed to the distinctive absorption bands at 3902.5 cm^{-1} , 3846.6 cm^{-1} , and 3749.7 cm^{-1} .

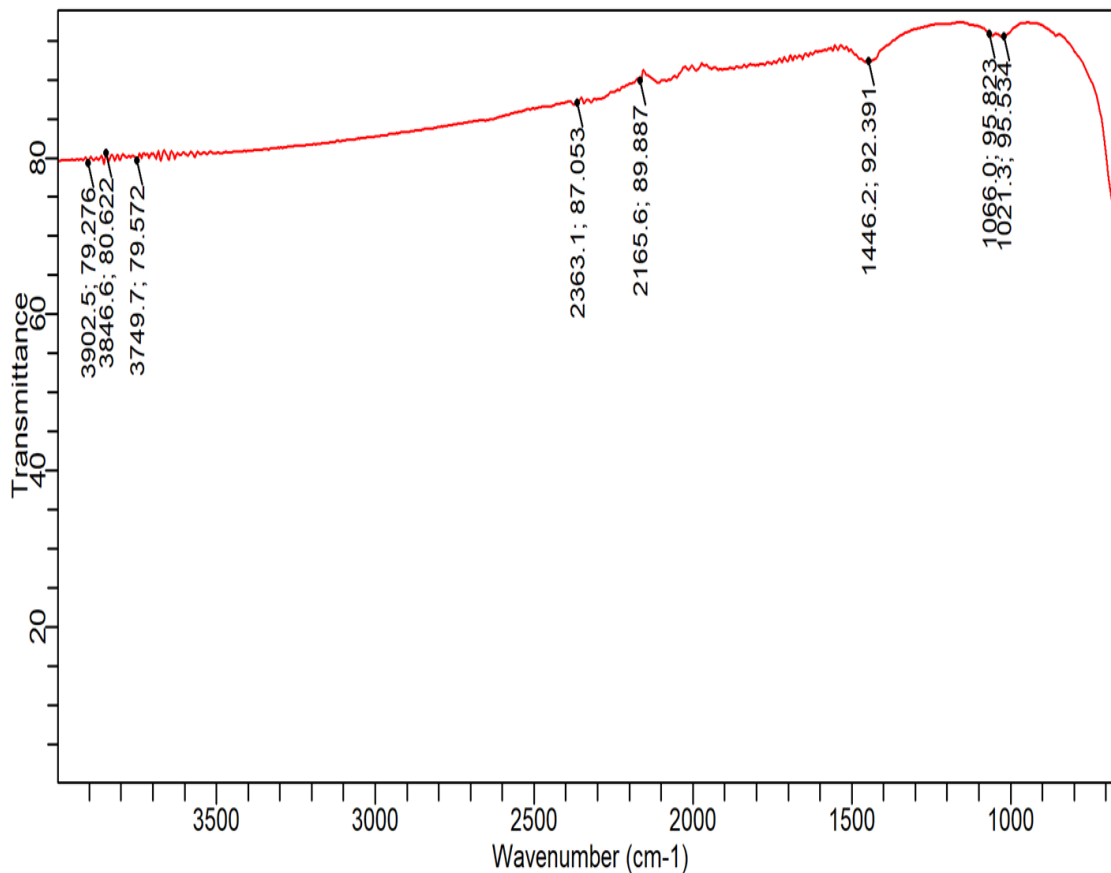


Fig. 5: FTIR spectra of the $\text{Ba}_{0.91}\text{Ca}_{0.09}\text{Sn}_{0.01}\text{Ti}_{0.9}\text{O}_3$ ceramic

Dielectric properties

Fig 6 shows the plot of the dielectric permittivity as a function of temperature from room temperature (25°C to 600°C) and in the frequency range of 5 kHz to 2 MHz for the $\text{Ba}_{0.91}\text{Ca}_{0.09}\text{Sn}_{0.01}\text{Ti}_{0.9}\text{O}_3$ ceramic. Fig 6 shows two main dielectric anomalies within the temperature range, both of which are caused by phase transitions. At approximately 150°C, the first maximum corresponds to a phase transition from the orthorhombic ferroelectric phase T_{R-O} . At approximately 500°C, the second maximum occurs, corresponding to a phase change from orthorhombic to tetragonal ferroelectric phase T_{O-T} . These dielectric phase transitions are critical for energy storage in capacitors. The T_{R-O} transition enhances dielectric permittivity due to lattice distortion, enabling higher charge storage, while T_{O-T} stabilizes the material's thermal response, reducing losses at elevated temperatures. These transitions align with the operational requirements of multilayer ceramic capacitors (MLCCs), where high permittivity and thermal stability are essential. The relaxation behaviour observed (Fig. 6) minimizes hysteresis losses, improving energy efficiency.

Phase transitions in Fig. 6 were identified to pinpoint inflection points. Error margins for T_{R-O} and

T_{O-T} are $\pm 5^\circ\text{C}$, based on triplicate measurements. The transitions align with La-doped BiFeO_3 studies [24], where analogous phase shifts improved thermal stability. Compared to barium titanate, these two phases demonstrate a better dielectric relaxation phenomenon in the produced $\text{Ba}_{0.91}\text{Ca}_{0.09}\text{Sn}_{0.01}\text{Ti}_{0.9}\text{O}_3$ ceramic. To make high-capacitance multilayer ceramic capacitors (MLCCs), the ceramic capacitor industry requires very fine barium titanate powders with high dielectric constants and dielectric relaxation, in which the value of the synthesized $\text{Ba}_{0.91}\text{Ca}_{0.09}\text{Sn}_{0.01}\text{Ti}_{0.9}\text{O}_3$ ceramic is advantageous. Dielectric relaxation is a temporary change in a material's dielectric constant induced by a delay in molecular polarization in response to a changing electric field inside a capacitor acting as a dielectric medium. The total capacitance of a parallel-plate capacitor is increased by the presence of a dielectric in the gap. The size effect, on the other hand, is known to show that the dielectric constant decreases with decreasing particle size and disappears below a certain critical size due to a phase change from tetragonal to cubic in conjunction with particle size reduction. Physical characteristics such as chemical purity, surface flaws, particle size, and sintering conditions all affect this crucial particle size, as does the particle size of the produced $\text{Ba}_{0.91}\text{Ca}_{0.09}\text{Sn}_{0.01}\text{Ti}_{0.9}\text{O}_3$ ceramic, which is $1.64\ \mu\text{m}$ [27].

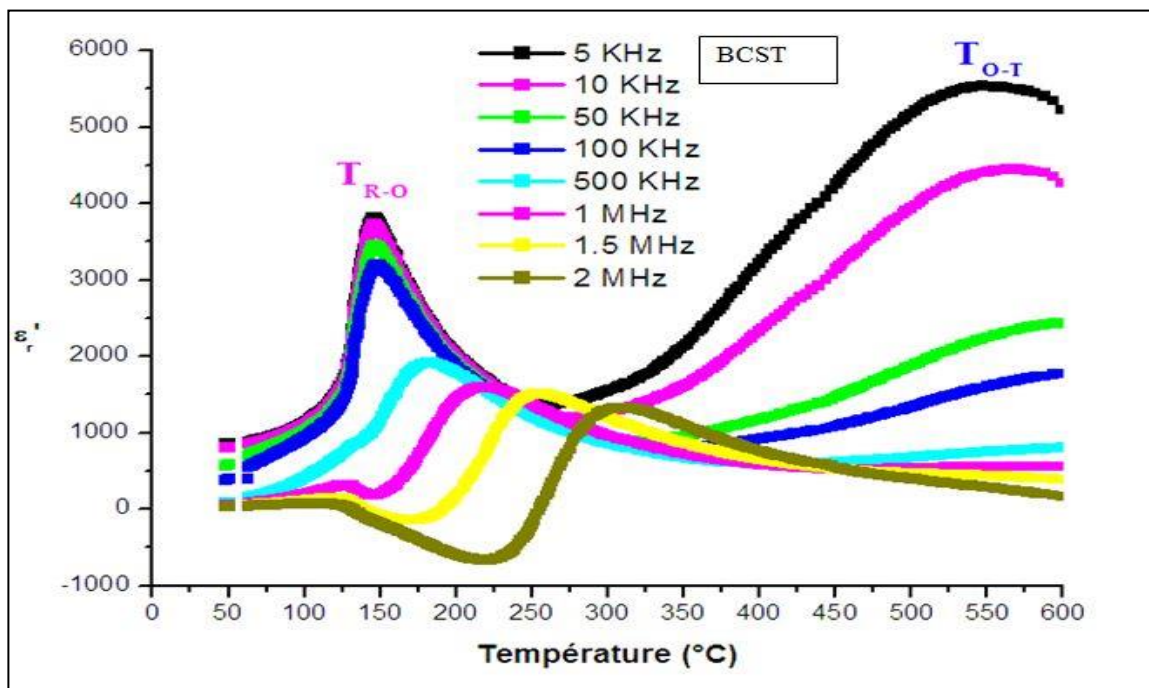


Fig. 6: Temperature dependence of the dielectric permittivity of the $\text{Ba}_{0.91}\text{Ca}_{0.09}\text{Sn}_{0.01}\text{Ti}_{0.9}\text{O}_3$ ceramic.

Conclusions

This study introduces Sn/Ca co-doping to stabilize tetragonal BaTiO₃ with dual phase transitions, achieving enhanced dielectric relaxation. Solid-state synthesis was employed to make the Ba_{0.91}Ca_{0.09}Sn_{0.01}Ti_{0.9}O₃ ceramic at a temperature of 1100°C. XRD, SEM, EDS and FTIR were used to characterize the synthesized ceramic, while the dielectric properties as a function of temperature were investigated with an Agilent E4980A Precision LCR meter. The presence of a lead-free crystalline ceramic with a tetragonal perovskite structure is confirmed by the XRD results. The presence of Sn, Ba, Ti, Ca, O, C, Pd, and Au was determined using the EDS spectra of the BCST ceramic. The grains have a relatively inhomogeneous shape and porosity, with a no uniform distribution of grains and a coexistence of tiny and large grains with an average grain size of 1.64 μm, according to the SEM results. The existence of two phase transitions, T_{R-O} and T_{O-T}, as well as a relaxation behaviour that favours their implementation in a ceramic capacitor, can be seen in the change in dielectric characteristics as a function of temperature. For future work, we hope to optimize Sn/Ca ratios to suppress secondary phases, test MLCC prototypes under high-field conditions and investigate co-doping with rare earths (e.g., Nd, Sm) for low-temperature applications.

Acknowledgements

The authors thank the Departments of Physics and Chemical Engineering at AEFUNAI for carrying out the materials synthesis, as well as Umaru Musa Yaraduwa University, Katsina, University of Kwazulu-Natal, South Africa, and Usmanu Danfodiyo University, Sokoto, Nigeria, for carrying out the characterizations.

References

1. B Supriya, M Ashutosh and M J Kanaka, Structural, optical and dielectric properties of Nickel substituted Barium Titanate ceramics, *J. Phys. Conf. Ser.* **755**012048 (2016).
2. N Shaban and M Bahar, Synthesis and Characterization of Fe and Ni Co-Doped Ba_{0.6}Sr_{0.4}TiO₃ Prepared by Sol-Gel Technique, *JTCS.* **4** 1 (2017).
3. N. Gouitaa, T Lamcharfi, L Bouayad, F Abdi, O Mohamed and M Sajieddine, The Study of Structure and Transitional Phases in Ba_{0.95}Bi_{0.05}Ti_{1-x}XFexO₃ Ceramics Synthesized by Solid State Route, *Iran. J. Mater. Sci. Eng.* **18** 1 (2021)
4. O L Alderman, C Benmore, J Neufeind, A Tamalonis and R Weber, Molten barium titanate: a high-pressure liquid silicate analogue, *J. Phys. Condens. Matter.* **31** 20 (2019).
5. E Aksel and J L Jones, Advances in lead-free piezoelectric materials for sensors and actuators, *Sensors.* **10** 1935 (2010).
6. A Frattini, A Di-Loreto, O deSanctis and E Benavidez, BCZT ceramics Prepared from activated powders, *Procedia Material Science.* **1** 359 (2012).
7. N Gouitaa, T Lamcharfi, L Bouayad, F Abdi, M N Bennani, M, Structural and dielectric properties of Ba_{0.95}Bi_{0.05}Ti_{1-x}FexO₃ ceramics at x=0.0,0.1 and 0.2 prepared by solid state method, *Mediterr. J. Chem.* **8** 220 (2019).
8. M M Vijatovic, J D Bobic and B.D Stojanovic, History and challenges of Barium Titanate: Part I, *Sci. Sinter.* **40** 55 (2008).
9. A Belkin, A Bezryadin, L Hendren and A Hubler, Recovery of Alumina Nanocapacitors after High and Low Voltage Breakdown, *Sci. Rep.* **7**, 932 (2017).
10. M Shi, J Zhong, R Zuo, Y Xu, L Wang, H Su and C Gu.), Effect of annealing processes on the structural and electrical properties of the lead-free thin films of (Ba_{0.9}Ca_{0.1})(Ti_{0.9}Zr_{0.1})O₃, *J. Alloys Compd.* **562** 116122 (2013).
11. S Maitra, M Banerjee, S Mukherjee and P K Singh, Synthesis and Characterisation of Cobalt Oxide Doped Barium Strontium Titanate, *J. Aust. Ceram.* **49** 79 (2013).
12. Z Lijuan, W Lihai, L Jiandang, C Bin, Z Minglei and Y Bangjia, Dielectric properties and structural defects in BaTi_{1-x}Sn_xO₃ ceramics, *J. Phys. Conf. Ser.* **443** 012014 (2013)
13. A K Nath, A Medhi, Effect of gamma ray irradiation on the piezoelectric and ferroelectric properties of bismuth doped barium titanate ceramics, *Indian J. Phys.* **89** 131 (2015)
14. U I Remy, T Louis-Pascal, L Franck, and M Pham-Thi 2017 IEEE International Ultrasonics Symposium (IUS), Sep 2017, Washington, DC, United States, ff10.1109/ULTSYM.2017.8091772ff.fhal-01705122 (2018).
15. G Najwa, L Taj-dine and B Lamfaddal, The Study of Structure and Transitional Phases in Ba_{0.95}Bi_{0.05}Ti_{1-x}XFexO₃ Ceramics Synthesized by Solid State Route, *Iran. J. Mater. Sci. Eng.* **18** 1 (2020).
16. U Ahmadu, A A Soje, A B Usman, A M Musa and K U Isah, Structural and microstructural study of gamma ray-irradiated co-doped barium titanate (Ba_{0.88} Ca_{0.12} Ti_{0.975} Sn_{0.025} O₃), *Process. Appl. Ceram.* **10**, 798 (2016).

17. G Julio, M D Merindano, M Canals and M Rallo, Image processing techniques to quantify micro projections on outer corneal epithelial cells, *J. Anat.* **212** 879 (2008)
18. W S Rasband. imagej USA: National institute of health 1 (2014). <http://imagej.nih.gov/ij/1997-2014>
19. T O Daniel, U E Uno K U, Isah and U Ahmadu, Tuning of SnS Thin Film Conductivity on Annealing in an open air environment for Transistor application, *EEJP*, **2**, 94-103. <https://doi.org/10.26565/2312-4334-2020-2-08>, *EEJP* **2** 94 (2020)
20. K Matsuura, T Hoshina, H Takeda, Y Sakabe and T Tsurumi, Effects of Ca substitution on room temperature resistivity of donor-doped barium titanate based PTCR ceramics, *J. Ceram. Soc. JAPAN*, **122**, 402 (2014)
21. N Medhi and A K Nath, Gamma ray irradiation effects on ferroelectric and piezoelectric properties of Barium Titanate Ceramics, *J. Mater. Eng. Perform.* **22** 2716 (2013).
22. A. K. Sahu, P. Mallick, S. K. Satpathy, and B. Behera, Effect on structural, electrical and temperature sensing behavior of neodymium doped bismuth ferrite, *Adv. Mater. Lett.*, (2021) <https://doi.org/10.5185/amlett.2021.071648>
23. H A Mady, XRD and Electric properties of lead barium titanate ferroelectric ceramic, *AJBAS* **5** 1472 (2011)
24. P. Mallick, A. K. Sahu, S. K. Biswal, S. K. Satpathy, and B. Behera, Effect on structural, electrical and temperature sensing behavior of neodymium doped bismuth ferrite, *Trans. Electr. Electron. Mater.*, **23** 522-534 (2022).
25. P. Mallick, S. K. Satpathy, and B. Behera, Study of Structural, Dielectric, Electrical, and Magnetic Properties of Samarium-Doped Double Perovskite Material for Thermistor Applications, *Braz. J. Phys.*, **52** 187 (2022). <https://doi.org/10.1007/s13538-022-01190-9>
26. P. Mallick, R. Patra, D. Mohanty, et al Development and characterization of copper doped perovskite-polymer composite through high-temperature technique, *Sādhanā*, **47** 134 (2022). <https://doi.org/10.1007/s12046-022-01904-4>
27. S Yun, X Wang, B Li and D Xu, Dielectric properties Ca-substituted barium strontium titanate ferroelectric ceramics, *Solid State Commun.* **143** 461(2007).